

Article

Metal-Rich Metallaboranes: Synthesis, Structures and Bonding of Bi- and Trimetallic Open-Faced Cobaltaboranes

Kriti Pathak ¹, Chandan Nandi ¹, Jean-François Halet ^{2,*} and Sundargopal Ghosh ^{1,*}

¹ Department of Chemistry, Indian Institute of Technology Madras, Chennai 600036, India; kritipathak04@gmail.com (K.P.); chandannandi.chem458@gmail.com (C.N.)

² CNRS—Saint-Gobain—NIMS, IRL 3629, Laboratory for Innovative Key Materials and Structures (LINK), National Institute for Materials Science (NIMS), Tsukuba 305-0044, Japan

* Correspondence: jean-francois.halet@univ-rennes1.fr (J.-F.H.); sghosh@iitm.ac.in (S.G.); Tel.: +91-44-225-742-30 (S.G.)

Abstract: Synthesis, isolation, and structural characterization of unique metal rich diamagnetic cobaltaborane clusters are reported. They were obtained from reactions of monoborane as well as modified borohydride reagents with cobalt sources. For example, the reaction of $[\text{Cp}^*\text{CoCl}]_2$ with $[\text{LiBH}_4\cdot\text{THF}]$ and subsequent photolysis with excess $[\text{BH}_3\cdot\text{THF}]$ (THF = tetrahydrofuran) at room temperature afforded the 11-vertex tricobaltaborane *nido*- $[(\text{Cp}^*\text{Co})_3\text{B}_8\text{H}_{10}]$ (**1**, $\text{Cp}^* = \eta^5\text{-C}_5\text{Me}_5$). The reaction of $\text{Li}[\text{BH}_2\text{S}_3]$ with the dicobaltoctaborane(12) $[(\text{Cp}^*\text{Co})_2\text{B}_8\text{H}_{10}]$ yielded the 10-vertex *nido*-2,4- $[(\text{Cp}^*\text{Co})_2\text{B}_8\text{H}_{12}]$ cluster (**2**), extending the library of dicobaltadecaborane(14) analogues. Although cluster **1** adopts a *classical* 11-vertex-*nido*-geometry with one cobalt center and four boron atoms forming the open pentagonal face, it disobeys the Polyhedral Skeletal Electron Pair Theory (PSEPT). Compound **2** adopts a perfectly symmetrical 10-vertex-*nido* framework with a plane of symmetry bisecting the basal boron plane resulting in two $\{\text{CoB}_3\}$ units bridged at the base by two boron atoms and possesses the expected electron count. Both compounds were characterized in solution by multinuclear NMR and IR spectroscopies and by mass spectrometry. Single-crystal X-ray diffraction analyses confirmed the structures of the compounds. Additionally, density functional theory (DFT) calculations were performed in order to study and interpret the nature of bonding and electronic structures of these complexes.

Keywords: cobaltaborane; decaborane; eleven-vertex cluster; *nido* cluster; metallaborane; mixed-metal cluster; ten-vertex cluster

Citation: Pathak, K.; Nandi, C.; Halet, J.-F.; Ghosh, S. Metal-Rich Metallaboranes: Synthesis, Structures and Bonding of Bi- and Trimetallic Open-Faced Cobaltaboranes. *Inorganics* **2021**, *9*, 28. <https://doi.org/10.3390/inorganics9040028>

Received: 22 March 2021

Accepted: 6 April 2021

Published: 13 April 2021

Publisher's Note: MDPI stays neutral with regard to jurisdictional claims in published maps and institutional affiliations.



Copyright: © 2021 by the authors. Licensee MDPI, Basel, Switzerland. This article is an open access article distributed under the terms and conditions of the Creative Commons Attribution (CC BY) license (<http://creativecommons.org/licenses/by/4.0/>).

1. Introduction

Polyhedral cage expansion for the synthesis of large clusters has been the objective of boron-rich metallaborane and metallacarborane chemistry over the last six decades [1–6]. Molecular boron-rich clusters have found their place in many fields ranging from ceramics and polymers to boron neutron capture therapy and nanomaterials [7–10]. Those applications along with more fundamental studies of their specific and somewhat unique bonding and electronic structures have been the driving force towards the development of this chemistry [7,11,12]. In particular, following the pioneering work of Hawthorne et al. [13], several groups such as those of Evans [14], Welch [15], Xie [16,17], and ours [18–20] have contributed in enriching the library of the large 12–16 vertex single cage polymetalla(hetero)borane clusters over the years. The already extensive array of metallaborane clusters continues to grow in direct proportion with the advent of novel synthetic methods [9,11,17,21–33]. However, it is difficult to come up with an integrated scheme aimed at the synthesis of polyhedra bearing definite geometry and composition. This is largely due to the undefined and uncontrolled nature of cluster growth from metal synthons or small preformed clusters. Even the most sought-after strategies like

condensation involving monoborane reagents, insertion or fragmentation involving borane or metal carbonyl fragments and cluster fusion [34] rarely exhibit metallaboranes with a high metal-to-boron ratio [35–39].

Among the several strategies aimed towards cluster expansion that have been conceived over the years, the reaction of cyclopentadienyl halides or hydrides with monoborane reagents such as $\text{BH}_3\cdot\text{THF}$ (THF = tetrahydrofuran), $[\text{BHCl}_2\cdot\text{SMe}_2]$, or $[\text{LiBH}_4\cdot\text{THF}]$, is a strategy that has been thoroughly optimized [40,41] and has proven to be very useful for yielding a variety of higher vertex metallaborane clusters adopting unique polyhedral cage geometries and structural features [41–45]. Although, in most cases, the metallaboranes are generated in small yields with a low metal-to-boron ratio, it was the strategy that involved pyrolyzing $[\text{Cp}^*\text{RhCl}_2]_2$ in large excess of $[\text{BH}_3\cdot\text{THF}]$, that allowed us to isolate 15- and 16-vertex rhodaborane clusters [18]. Although fused clusters [46] or single cage clusters bearing 5–11 vertices are reported with the cobalt system [20,46–52], isolation of analogous single cage supraicosahedral cobaltaboranes has not been successful up until now despite the fact that both rhodium and cobalt are group-9 metals. Indeed, our recent reports include the formation of a range of high-nuclearity cobaltaborane clusters, such as the hypoelectronic 9-vertex *closo*- $[(\text{Cp}^*\text{Co})_2\text{B}_7\text{H}_6\text{OMe}]$, hypoelectronic octadecahedral 11-vertex *closo*- $[(\text{Cp}^*\text{Co})_3\text{B}_8\text{H}_7\text{R}]$ (R = H or Me), and icosahedral 12-vertex *closo*- $[(\text{Cp}^*\text{Co})_3\text{B}_8\text{H}_8\text{S}]$ species obtained from the reaction of $[\text{Cp}^*\text{CoCl}]_2$ with $[\text{LiBH}_4\cdot\text{THF}]$ and subsequent thermolysis with 2-mercaptobenzothiazole in toluene [50]. Our renewed quest for higher nuclearity cobaltaboranes made us look for modified synthetic strategies and although the objective of isolating a single cage supraicosahedral cobaltaborane was not achieved, the treatment of $[\text{Cp}^*\text{CoCl}]_2$ with $[\text{LiBH}_4\cdot\text{THF}]$ followed by photolysis with excess $\text{BH}_3\cdot\text{THF}$ afforded the 11-vertex-(hyper)*nido*- $[(\text{Cp}^*\text{Co})_3\text{B}_8\text{H}_{10}]$ cluster (**1**). Group-9 metallaboranes have continually monopolized the field not only for novelty in geometries but also for the possibility to draw on the open cage molecules like $[(\text{Cp}^*\text{M})_2\text{B}_6\text{H}_{10}]$ [M = Co and Rh] and $[(\text{Cp}^*\text{Rh})_2\text{B}_8\text{H}_{12}]$ for further reactivities [53]. We have ourselves contributed significantly to this area by enriching the library of mono- and dicobaltadecaborane(14) analogues in the past [50–52]. Most recently, we have explored and reported the chemistry of dicobaltoctaborane(12) with chalcogenated borohydride, $\text{Li}[\text{BH}_2\text{E}_3]$ [E = S, Se, or Te] which resulted in the characterization of novel chalcogenated analogues of dicobaltadecaborane(14) [54]. Careful analysis of the reaction between $[(\text{Cp}^*\text{Co})_2\text{B}_6\text{H}_{10}]$ and $\text{Li}[\text{BH}_2\text{S}_3]$ led to the isolation of 2,4- $[(\text{Cp}^*\text{Co})_2\text{B}_8\text{H}_{12}]$ (**2**), a new dicobaltadecaborane(14) analogue. The main results are presented in this article.

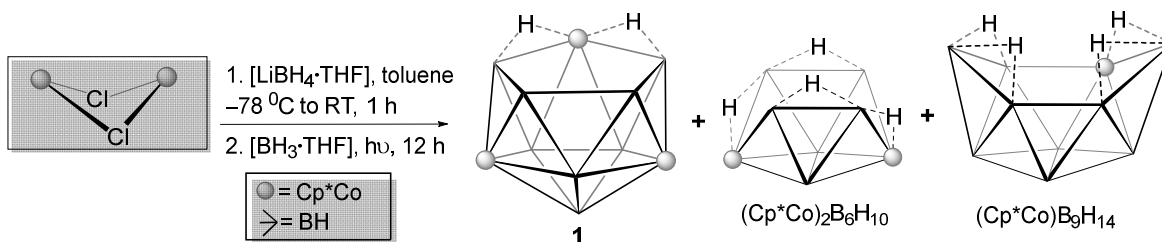
2. Results and Discussion

2.1. Reaction of $(\text{Cp}^*\text{CoCl})_2$ with $[\text{LiBH}_4\cdot\text{THF}]$ and $[\text{BH}_3\cdot\text{THF}]$

The reaction of $[\text{Cp}^*\text{CoCl}]_2$ with an eight-fold excess of $[\text{LiBH}_4\cdot\text{THF}]$ followed by photolysis with excess of $\text{BH}_3\cdot\text{THF}$ at room temperature for 16 h led to the formation of a green crystalline solid in 10% yield which was characterized as a novel open-faced 11-vertex cobaltaborane, (hyper)*nido*- $[(\text{Cp}^*\text{Co})_3\text{B}_8\text{H}_{10}]$ (**1**). The reaction also yielded cobaltaboranes reported in the recent past like $[(\text{Cp}^*\text{Co})_2\text{B}_6\text{H}_{10}]$ and $[(\text{Cp}^*\text{Co})\text{B}_9\text{H}_{14}]$ [52] (Scheme 1) and a few other compounds which could not be isolated due to lesser yields and transient natures. Preparative thin-layer chromatography (TLC) allowed separation of **1** from the reaction mixture and hence enabled the characterisation of the pure compound. Multinuclear NMR (see Figures S1–S4 for spectra) and IR spectroscopies and solid-state structure determination by X-ray diffraction analysis helped establish the composition and structure of **1**. A detailed account of the spectroscopic and structural characterizations of **1** follows.

$[(\text{Cp}^*\text{Co})_3\text{B}_8\text{H}_{10}]$, **1**. The room temperature $^{11}\text{B}\{^1\text{H}\}$ NMR of **1** shows the presence of four resonances between 71.4 and 19.7 ppm. The $^1\text{H}\{^{11}\text{B}\}$ NMR spectrum of **1** suggests the existence of two different Cp^* environments appearing at 1.9 and 1.7 ppm with a relative ratio of 1:2. This is also corroborated by the $^{13}\text{C}\{^1\text{H}\}$ NMR spectrum. In addition to the

chemical shifts corresponding to B- H_t protons, the $^1\text{H}\{^{11}\text{B}\}$ NMR spectrum also shows a sharp upfield resonance in the hydride region at $\delta = -20.43$ ppm which may typically be arising due to two equivalent Co- H -B protons. The infrared (IR) spectrum shows broad bands around 2438 cm^{-1} owing to stretching frequencies of the terminal B- H_t bonds. Although the spectroscopic data indicated the formation of a large cluster, they were not sufficient to help conceptualize the actual identity of **1**. A clear identification was obtained only after the crystal structure determination of **1** which was carried out with crystals obtained by slow evaporation of a concentrated hexane/ CH_2Cl_2 (90:10) solution of **1** kept at $-10\text{ }^\circ\text{C}$.



Scheme 1. Synthesis of the open-faced tricobaltaborane cluster **1**.

The molecular structure of **1** (Figure 1) adopts a classical 11-vertex *nido* core that can be formally generated by the removal of an apical vertex of the ubiquitous 12-vertex icosahedron (Figure 2). The molecule has two minor disordered components with atoms B8 and B8', each with 50% occupancy. Despite the lack of precision in some of the bond distances and angles of the cluster owing to the restraints set to resolve this disorder, the crystallographic data reasonably allow a clear determination of the structure. Only one of the residues (with B8') is discussed and shown in Figure 1. The five atoms of the open face (Co1, B4, B5, B7, and B8') of the cluster are four-connected vertices while the remaining six ones are all five-connected vertices (Figure 1). This is in agreement with the NMR results discussed above which indicate that the higher chemical shifts in the ^{11}B NMR spectrum corresponds to the high connected B atoms with the chemical shifts for B1 and B2 accidentally eclipsing at 71.4 ppm thus displaying four resonances in the ratio 2:2:2:2. A crystallographic mirror plane passing through the atoms Co1, B1, and B2 bisects the molecule into two symmetrical entities, thereby rendering the chemical environments of Cp^* ligands attached to Co2 and Co3 as equivalent.

The polyhedral cage geometry of cluster **1** looks reminiscent of that of classical 11-vertex *nido* geometry of related clusters such as $[\text{C}_2\text{B}_9\text{H}_{11}]^{2-}$, $[(\text{Cp}^*\text{Rh})_3\text{B}_8\text{H}_9(\text{OH})_3]$ [55], $[\textit{nido-7,8,9-PC}_2\text{B}_8\text{H}_{11}]$ [56], $[\textit{8,8-}\eta^2\text{-}\{\eta^2\text{-}(\text{BH}_3)\text{-dppm}\}\textit{-nido-8,7-RhSB}_9\text{H}_{10}]$ [57], $[\textit{9,9-}\eta^2\text{-}\{\eta^2\text{-}(\text{BH}_3)\text{-dppm}\}\textit{-nido-9,7,8-RhC}_2\text{B}_8\text{H}_{11}]$ [57], and $[(\mu\text{-PPh}_2)(\text{PPh}_3)_2\text{Pt}_2\text{B}_9\text{H}_6(\text{O}^i\text{Pr})_3]$ [58] for instance which all possess 13 skeletal electron pairs (SEP), i.e., $(n + 2)$ SEPs if n is the number of occupied vertices according to the Polyhedral Skeletal Electron Pair Theory (PSEPT) [59]. Interestingly, however, with only 12 skeletal electron pairs (SEPs), cluster **1** is two electrons short of the formal $(n + 2)$ SEP count expected for *nido* clusters as required by the PSEPT [59]. As stated earlier, in addition to the BH_t and Cp^* protons, the $^1\text{H}\{^{11}\text{B}\}$ NMR spectrum shows the presence of only a single resonance for two bridging Co- H -B protons. The presence of two B- H -B protons which would have afforded a *nido* species with the “expected” electron count could not be traced from ^1H NMR.

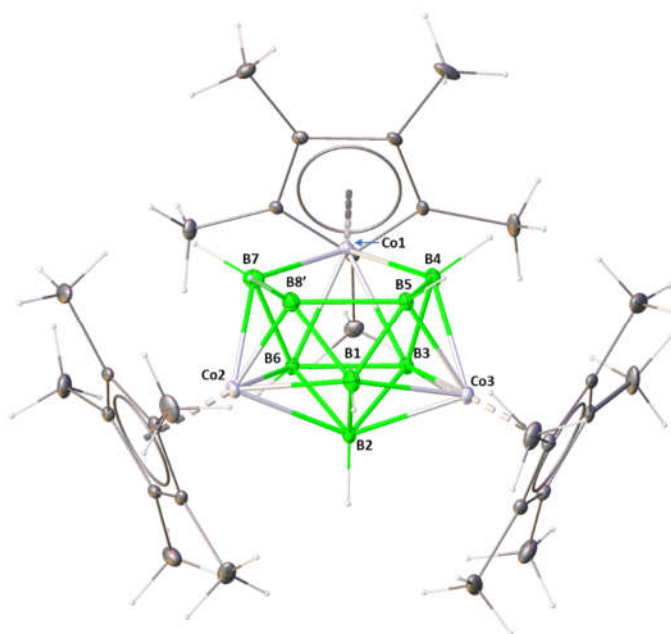


Figure 1. Molecular structure and atom labels of one of the residues of **1**. Selected bond lengths (Å) and bond angles (°) of **1**: B1–B2 1.82(2), B1–Co3 2.051(14), B1–Co2 2.063(16), B2–Co3 2.084(13), B6–B7 1.78(2), B4–Co1 2.067(14), B7–Co1 2.030(14), B7–B8'–B5 113.0(17), and B7–Co1–B4 87.4(6). Co–H–B bridging hydrogens could not be located.

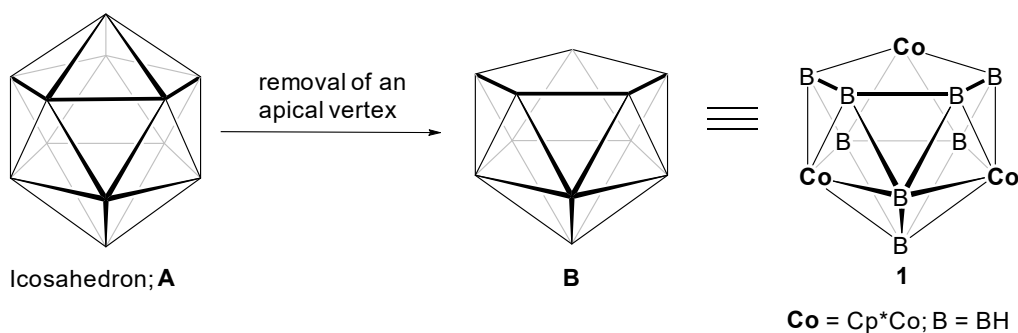


Figure 2. Schematic representation of stepwise generation of the cluster framework of **1** (**B**) from an icosahedron (**A**).

To the best of our knowledge cluster **1** is the first example of electron-poor 11-vertex–12-SEP (hyper)nido species of this kind in the metallaborane cluster domain. Nevertheless, isoelectronic and isostructural examples are known in metallacarborane chemistry. Indeed, cluster **1** can be compared both electronically and structurally to some 11-vertex–12-SEP nido clusters such as [9,9-*L*₂-nido-9,7,8-MC₂B₈H₁₁] (**I**: L = PPh₃, M = Ir; **II**: L = PEt₃, M = Rh) [60] and [8,8-(PPh₃)₂-nido-8,7-RhSB₉H₁₀] (**III**) [61,62] (Chart 1). 11-vertex–12-SEP metalla(hetero)borane compounds exist such as [1-PPh₃-{1,3-(μ-dppm)}-isonido-1,2-RhSB₉H₈] [**IV**; dppm = CH₂(PPh₂)₂] [63,64], or [1,1,1-(H)(PMe₃)₂-isonido-1,2-IrSB₉H₉] (**V**) [65] (Figure 3), but they are not isostructural with **1**. While the latter is generated from the icosahedron by removing one vertex (Figure 2), the geometry reported for the 11-vertex *isonido* clusters [63–65] is derived from an 11-vertex octadecahedron by the removal of one connectivity of the apical vertex thereby generating a distorted quadrilateral open face (**D**; top of Figure 3).

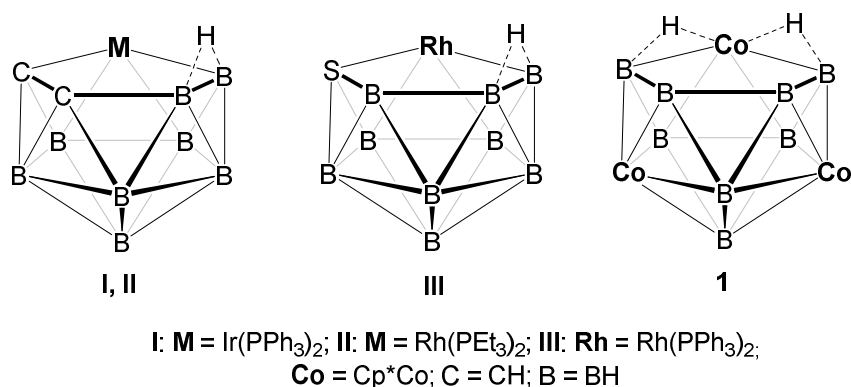


Chart 1. Examples of 11-vertex-12-SEP (skeletal electron pairs) *nido*-metalla(hetero)borane clusters.

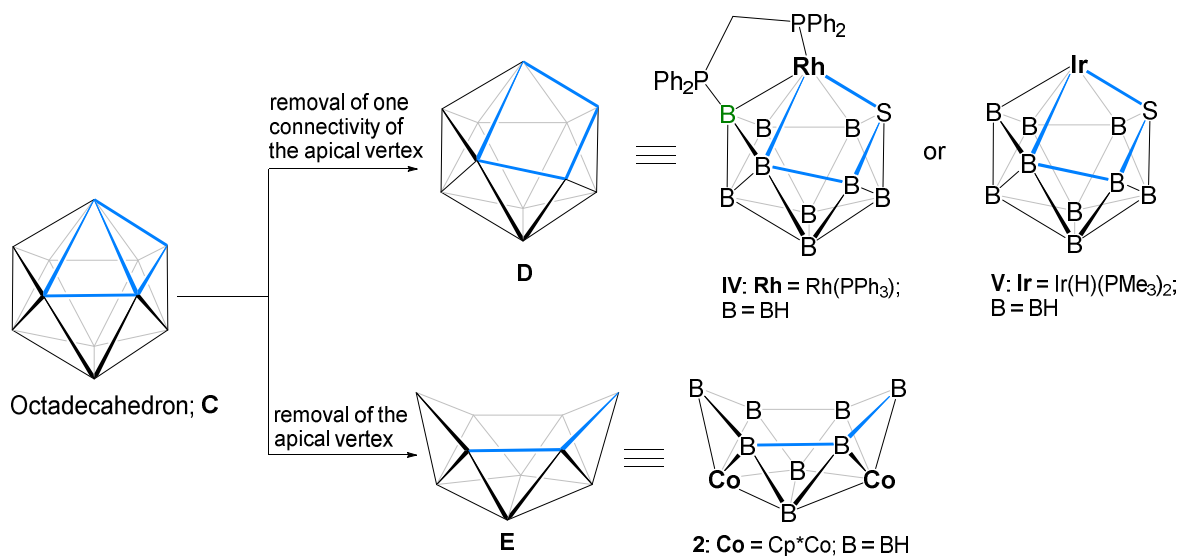


Figure 3. Schematic representation of stepwise generation of the 11-vertex *isonido* (**D**) and 10-vertex *nido* (**E**) cluster frameworks from an octadecahedron (**C**) and their examples.

Density functional theory (DFT) calculations were carried out at the B3LYP/LANL2DZ level of theory (see computational details in Section 3) on model compound **1'** (Cp analogue of **1**) to analyse the electronic structure and nature of bonding in the electron deficient molecule **1**. Optimized bond distances in **1'** are in accordance with those experimentally measured for the solid-state structure of **1** (Table S1). The molecular orbital (MO) analysis of **1'** (Table S2) shows a large energy gap of 2.79 eV between the highest occupied molecular orbital (HOMO) and the lowest unoccupied molecular orbital (LUMO) in agreement with the electron count of 12 SEPs and the fact that only two bridging hydrogen atoms are present in the structure. The HOMO of **1'** is mainly localized on the metal centres and the five-connected inner-core boron atoms, whereas the LUMO is predominantly localized on the metal centres with considerable participation of the boron atoms of the open face of the cluster (Figure 4). We may wonder if cluster **1** could be reduced and reach the expected count of 13 SEPs to obey the PSEPT. It turns out that the LUMO + 1 is energetically close to the LUMO, separated only by 0.4 eV. This indicates that reduction of **1** is unlikely.

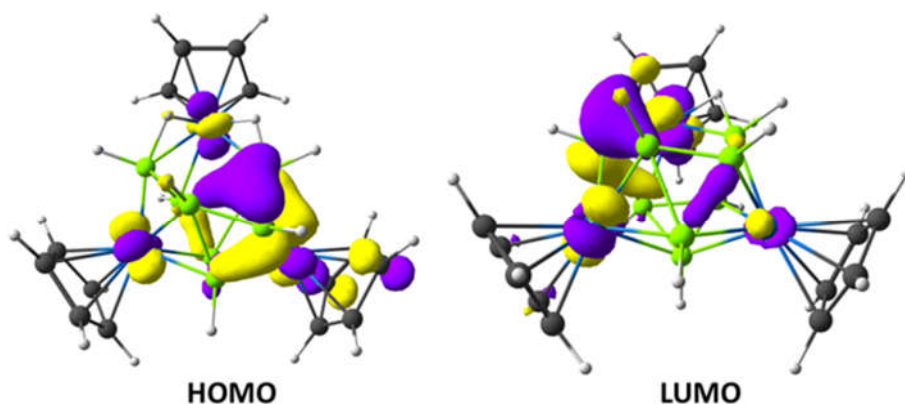
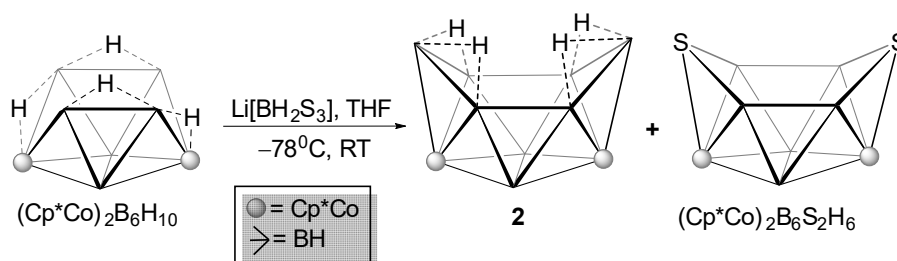


Figure 4. Frontier molecular orbitals of **1'**. Contour value: ± 0.05 [e/bohr³]^{1/2}.

2.2. Reactivity of [(Cp*Co)₂B₆H₁₂] with Li[BH₂S₃]

Reactions of the open-cage dicobaltoctaborane(12) analogue [(Cp*Co)₂B₆H₁₂] with chalcogenated borohydride Li[BH₂E₃] (E = S, Se, or Te) which were recently carried out in our group, resulted in the formation of novel chalcogenated analogues of dicobaltadecaborane(14), namely [(Cp*Co)₂B₆E₂H₆] (E = S, Se, or Te) [54]. The room temperature reaction between [(Cp*Co)₂B₆H₁₂] and Li[BH₂S₃] yielded another compound which could not be isolated earlier due to less yield. Performing the reaction at a larger scale followed by careful analysis of the reaction mixture led to the isolation of 2,4-[(Cp*Co)₂B₈H₁₂] (**2**), i.e., a novel dicobaltadecaborane(14) analogue (Scheme 2). This compound was characterized by ¹H, ¹¹B{¹H} and ¹³C{¹H} NMR (Figures S5–S8) and IR spectroscopies, mass spectrometry (Figure S9), and single-crystal X-ray diffraction analysis.



Scheme 2. Synthesis of a symmetric dicobaltaborane analogue of decaborane(14).

Dicobaltadecaborane(14) analogue, **2**. Cluster **2** was isolated as a yellow solid in 15% yield. The mass spectrometric data for **2** showed molecular ion peaks at m/z 487.2692 which corresponds to the molecular formula $[\text{C}_{20}\text{H}_{42}\text{B}_8\text{Co}_2]^+$. The ¹¹B{¹H} NMR showed chemical shifts at $\delta = 26.6$, 11.4, and 5.6 ppm, whereas ¹H NMR showed a single chemical shift for 30 Cp* protons at $\delta = 1.69$ ppm, and additionally, chemical shifts at $\delta = 4.38$, 2.94, and 2.31 ppm which correspond to B-H_{*t*} protons. A distinct up-field resonance was observed at $\delta = -4.25$ ppm which may be assigned to four equivalent B-H-B bridging protons. The chemical shifts displayed in the ¹³C{¹H} NMR spectrum also corroborated with a single Cp* environment in the molecule. The infrared (IR) spectrum showed broad bands centered around 2493 cm⁻¹ owing to stretching frequencies of the terminal B-H bonds.

Slow evaporation of a concentrated hexane/CH₂Cl₂ (80:20) solution of **2** kept at -10 °C yielded crystals suitable for X-ray diffraction analysis. The solid-state X-ray structure of **2** (Figure 5), determined by single-crystal X-ray diffraction measurements clearly shows that it is a 10-vertex open *nido*-dicobaltaborane which is in absolute agreement with the

spectroscopic as well as mass spectrometric data. It is apparent from its solid state X-ray structure that compound **2** adopts the same structural arrangement as the symmetric dimetalla *nido*-2,4-[(Cp**M*)₂B₈H₁₂] (*M* = Rh and Ir) [27,55] previously reported, analogues of decaborane(14). In the structure, a crystallographic mirror plane including the B6–B8 vector bisects the molecule into two equivalent {CoB₃} units. As a result, the two Co atoms that reside on either side of the crystallographic mirror plane are chemically equivalent and hence correspond to the presence of single Cp* environment in the ¹H and ¹³C{¹H} NMR spectra. The bridging hydrogen atoms lie on the open face of the six-membered ring and their presence is confirmed both by ¹H NMR and X-ray diffraction studies. We noted that the average B–B bond length in **2** is somewhat shorter as compared to the Rh and Ir analogues [27,55] and follows the trend (Co < Rh < Ir) down the triad. A {Cp*Co} unit being isolobal with a BH unit, the cluster is isostructural and isoelectronic with *nido*-decaborane(14) which can be generated from the removal of the six-connected apical vertex of an octadecahedron (see bottom of Figure 3). Indeed, **2** can be regarded as a 10-vertex *nido* metallaborane cluster with 12 SEPs, as expected according to the PSEPT. **2** is then a new member of the series of ten-vertex–12-SEP polyhedral borane, carborane, or metallaborane clusters having the same SEP count and geometry. We have tried to compare its structural data and chemical shift values with a set of comparable cobaltaboranes with the formal electron count of 12 SEPs (Table 1). The unique feature of this reaction here (Scheme 2) is the insertion of two BH units in octaborane(12) that leads to cluster growth from 8 to 10 vertices.

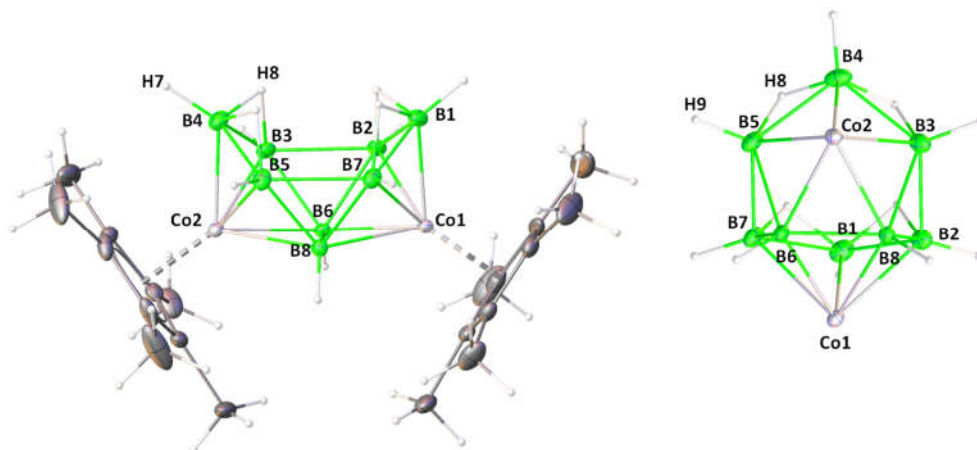


Figure 5. Molecular structure and atom labels for **2**: frontal view (left) and bottom angular view (right, Cp* ligands attached to Co are omitted for clarity). Selected bond lengths (Å) and bond angles (°): B1–Co1 1.972(5), B2–B3 1.971(7), B2–Co1 2.043(5), B3–B4 1.807(8), B3–Co2 2.043(4), B5–Co2 2.041(5), B7–Co1 2.046(4), B3–B2–Co1 115.5(2), B4–B3–B2 116.3(4), B3–B4–B5 103.9(3), and B2–Co1–B7 89.1(2).

Table 1. Selected structural and spectroscopic parameters of 10-vertex–12-SEP *nido*-cobaltaborane clusters. ^a

Geometry	$d(\text{B-B})_{\text{av}}$ [Å]	¹¹ B NMR (δ , ppm)	Ref.	Geometry	$d(\text{B-B})_{\text{av}}$ [Å]	¹¹ B NMR (δ , ppm)	Ref.
6-[(Cp*Co)B ₉ H ₁₃]	1.78	20.5, 15.4, 5.2, −1.2, −12.4, −29.8	[47]	3,5-[(Cp*Co) ₂ B ₈ H ₁₂]	1.80	42.4, 30.1, 25.3, 20.1, 9.1, 6.3, −1.2, −12.9	[52]
						49.9, 23.1, 19.4, 7.1, −7.1, −40.7	[47]
5-[(Cp*Co)B ₉ H ₁₃]	1.78	29.4, 27.1, 12.5, 4.1, 3.5, 1.7, −1.1, −14.5, −36.9	[52]	6-Cl-5,7-[(Cp*Co) ₂ B ₈ H ₁₂]	-		

	-	17.0, 14.6, 9.0, 1.7, -38.2	[49]		1.80	57.3, 24.4, 6.0, -7.4, 40.3	[47]
	1.78	11.7, 9.7, 0.28, -36.5	[66]		1.76	54.0, 29.7, 22.2, 8.7, 3.3, -40.1	[51]
	2.02	20.8, 2.3	[47]		1.81	26.6, 11.4, 5.6	This work

^a

In order to acquire an insight into the structure and bonding of **2**, we further did DFT calculations at the B3LYP/LANL2DZ level of theory (see computational details in Section 3 on model **2'** (Cp analogue of **2**) as well as on its group-9 metallaborane model analogues **3'** (Cp analogue of 2,4-[(Cp*Rh)₂B₈H₁₂]) and **4'** (Cp analogue of 2,4-[(Cp*Ir)₂B₈H₁₂]) for comparison. The optimized geometrical parameters obtained for **2'** compare fairly well with the corresponding crystallographically characterized data of **2** (Table S1). Additionally, the gauge-including atomic orbitals-density functional theory (GIAO-DFT) calculated ¹¹B chemical shift values agree well with those observed experimentally (Table 2) and are of sufficient accuracy to confirm assignments that are consistent with the empirical ones based simply on boron connectivity and environment (see above).

A molecular orbital analysis suggests a significant HOMO-LUMO energy gap (> 4 eV) for the three compounds in the order **2'** < **3'** < **4'** (Figure 6). Inspection of the nodal properties of the frontier MOs reveals that HOMOs weigh heavily on the respective metal centres, while the LUMOs are delocalized both on the metal centres and the five-connected inner-core boron atoms. Metal–metal Wiberg bond indices computed for **2'**, **3'**, and **4'** are very weak and close to each other (ca. 0.06), reflecting the nonappearance of bonding interaction between the metal centres in such species.

Table 2. Experimentally observed and calculated ¹H and ¹¹B chemical shifts for **2–4** species and **2'–4'** models, respectively.

Cluster	¹ H NMR δ (ppm)		¹¹ B NMR δ (ppm)		Ref.
	Expt.	Calc.	Expt.	Calc.	
2/2'	-4.25	-6.22	26.6, 11.4, 5.6	20.0, 11.0, 3.0	This work
3/3'	-3.52	-5.43	21.1, 9.4, 1.9	16.2, 6.5, 0.8	56 (expt.)
4/4''	-3.73	-5.45	1.8, -0.2, -12.9	7.3, -1.7, -11.0	27 (expt.)

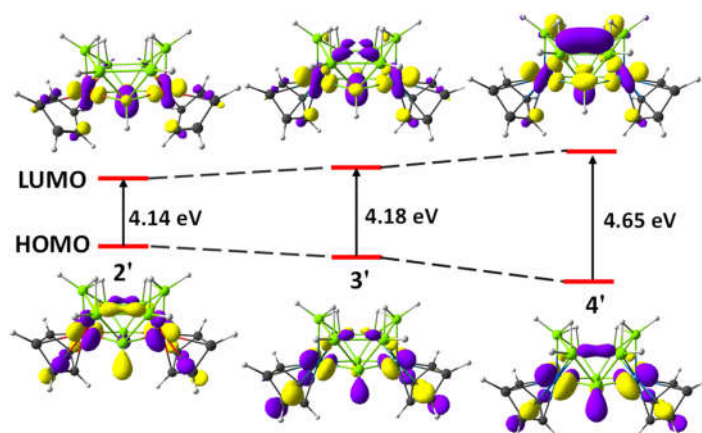


Figure 6. Frontier molecular orbital diagram of 2', 3', and 4' (see text). Contour value: ± 0.05 $[e/\text{bohr}^3]^{1/2}$.

3. Materials and Methods

3.1. General Methods and Instrumentation

All of the experiments were conducted under an argon atmosphere using standard Schlenk and glove-box techniques. Solvents were distilled prior to use under argon. Cp*H, CoCl₂, *n*-BuLi in hexane, LiBH₄ (2.0 M in THF), BH₃·THF, and S powder were used as received (Sigma Aldrich, Bangalore, India). (Cp*CoCl)₂ [67,68], [(Cp*Co)₂B₆H₁₀] [52], and Li[BH₂S₃] [69,70] were synthesized as per literature. Thin-layer chromatography, using silica gel TLC plates by Merck supported with 250- μm diameter aluminum, was done to separate the reaction mixtures. A 500 MHz Bruker FT-NMR spectrometer (Bruker, Billerica, MA, USA), JASCO FT/IR-4100 (JASCO, India) and Agilent Technologies: 6545-Q-TOF LC/MS (Agilent, Santa Clara, CA, USA) spectrometer were used respectively to record NMR, Infrared (IR) spectra, and ESI (Electrospray Ionization) mass. In ¹H NMR spectra, the chemical shifts for residual protons in the deuterated solvents were used as reference (CDCl₃, δ = 7.26 ppm, C₆D₆, δ = 7.16) while a sealed tube containing [Bu₄N(B₃H₈)] [71] in benzene-*d*₆ (δ_{B} , ppm, -30.07) was used as an external reference for ¹¹B{¹H} NMR spectra. The light source for the photoreaction described in this report was Oriel Instrument with a 500 W Hg/Xe arc lamp equipped with liquid and colored glass filters, irradiating at 280–780 nm.

Synthesis of 1: [Cp*CoCl]₂ (0.1 g, 0.22 mmol) was suspended in toluene (15 mL) in a flame-dried Schlenk tube and was cooled to -78°C, [LiBH₄·THF] (0.6 mL, 1.20 mmol) was added to it and the reaction mixture was allowed to warm slowly to room temperature and was left to stir for another hour. [BH₃·THF] (3 mL) was added to the reaction mixture and the resultant mixture was slowly warmed to room temperature was allowed to stir for 30 min, and finally kept for photolysis at room temperature for 12 h. After completion of the reaction (monitored by TLC), the solvent was removed under vacuum and the residue was dissolved in hexane and passed through Celite. The solvent was evaporated under vacuum and the residue was purified using preparative silica-gel TLC plates by eluting with hexane/CH₂Cl₂ (80:20) mixture that yielded green solid 1 (0.010 g, 10%) and known red solids [(Cp*Co)₂B₆H₁₀] (0.025 g, 24%), [(Cp*Co)₃B₄H₄] (0.018 g, 19%), and a few compounds which could not be isolated. The known cobaltaboranes were characterized with reference to their spectroscopic data reported earlier.

1: ¹¹B NMR (160 MHz, C₆D₆, 22 °C): δ = 71.5, 31.4, 24.5, 19.7 ppm; ¹H{¹¹B} NMR (500 MHz, C₆D₆, 22 °C): δ = 8.08 (br, 4H, BH_t), 5.16 (s, 2H, BH_t), 4.08 (s, 2H, BH_t), 1.94 (s, 15H, Cp*), 1.70 (s, 30H, Cp*) -20.43 (br, 2H, Co-*H*-B) ppm; ¹³C NMR (100 MHz, C₆D₆, 22 °C) = 96.0, 93.4 (C₅Me₅), 10.4, 9.6 ppm (C₅Me₅); IR (dichloromethane): $\bar{\nu}$ = 2438 (BH_t) cm⁻¹.

Synthesis of **2**: In a flame-dried Schlenk tube, [(Cp*Co)₂B₆H₁₀] (0.05 g, 0.107 mmol) was suspended in 5 mL of dry THF at room temperature. A freshly prepared solution of Li[BH₂S₃] in THF (10 mL, 0.428 mmol) was added dropwise to the red solution of [(Cp*Co)₂B₆H₁₀]. The reaction mixture was allowed to stir at room temperature for 24 h. The solvent was dried under vacuum and the residue was extracted into *n*-hexane/CH₂Cl₂ (85:15 *v/v*) mixture and passed through Celite. After removal of the solvent, the residue was subjected to chromatographic work-up by using TLC plates. Elution with an *n*-hexane/CH₂Cl₂ (85:15 *v/v*) mixture yielded the air-stable yellow solid (Compound **2**) (0.020 g, 38%) and the known compound [(Cp*Co)₂B₆H₆S₂] (0.016 g, 28 %) [57].

2: MS (ESI+): *m/z* calculated for C₂₀H₄₂B₈Co₂⁺ 487.2747, found 487.2692; ¹¹B NMR (160 MHz, CDCl₃, 22 °C): δ = 26.6, 11.4, 5.6 ppm; ¹H NMR (500 MHz, CDCl₃, 22 °C): δ = 4.38 (s, 2H, BH_t), 2.94 (s, 2H, BH_i), 2.31 (s, 4H, BH_i), 1.69 (s, 30H, Cp*), −4.25 (br, 4H, B-*H*-B) ppm; ¹³C NMR (100 MHz, CDCl₃, 22 °C) = 97.0 (C₅Me₅), 9.8 ppm (C₅Me₅); IR (dichloromethane): $\tilde{\nu}$ = 2493 (BH_t) cm^{−1}.

3.2. Single Crystal X-ray Diffraction Analysis

Crystallographic and structural refinement data for **1** and **2** are given in Table 3. Bruker AXS Kappa APEXII CCD diffractometer, (Bruker, Billerica, MA, USA) with graphite monochromatic Mo K_α (λ = 0.71073 Å) radiation at 296 K was used to collect and integrate crystal diffraction data. Heavy atom methods like SHELXT-2014 and SHELXS-97 [72–74] were used to solve the structures while SHELXL-2018 and SHELXL-2014 [73] were used for structure-refinements, respectively. Olex2 [75] was used for drawing molecular structures.

Table 3. Crystallographic and structural refinement data for **1** and **2**.

Compound	1	2
CCDC No.	2043679	2060786
Empirical formula	C ₃₀ H ₅₃ B ₈ Co ₃	C ₂₀ H ₄₂ B ₈ Co ₂
Formula weight	676.99	486.87
Crystal system	Triclinic	Monoclinic
Space group	<i>P</i> $\bar{1}$	<i>P</i> 2 ₁ / <i>n</i>
<i>a</i> (Å)	8.785 (4)	8.3902 (2)
<i>b</i> (Å)	11.638 (6)	40.6669 (12)
<i>c</i> (Å)	16.993 (9)	8.5097 (2)
α (°)	96.244 (18)	90
β (°)	96.56 (2)	119.0361 (11)
γ (°)	101.532 (18)	90
Volume (Å ³)	1675.6 (15)	2538.60 (12)
<i>Z</i>	2	4
ρ _{calc} (g/cm ^{−3})	1.342	1.274
μ (mm ^{−1})	1.487	1.312
F (000)	708	1024
2θ range for data collection (°)	3.6–44.9	2–50
Independent reflections	3990	4472
Final R indices [I ≥ 2σ (I)]	R ₁ = 0.0889, wR ₂ = 0.2412	R ₁ = 0.0439, wR ₂ = 0.0958
Parameters	452	329

3.3. Computational Details

Gaussian 09 program package [76] was used for geometry optimizations of all model clusters. Computations were done with the Cp ligands in place of Cp* to reduce the computational effort (for optimized model clusters see Figures S10–S13). Gas-phase optimizations without any solvent effect or symmetry constraints, were done with the

hybrid Becke–Lee–Yang–Parr (B3LYP) functional [77] in combination with the LANL2DZ (Los Alamos National Laboratory 2 Double-Zeta) basis set [78] for all the atoms from the EMSL (Environmental Molecular Sciences Laboratory) Basis Set Exchange Library [79]. Frequency calculations were carried out for all structures to check the nature of the stationary states and the absence of any imaginary frequency to confirm that the optimized geometries were genuine minima on the potential energy hypersurface. NMR chemical shifts were computed by employing the gauge-including atomic orbitals (GIAOs) method [80–82] using the optimized geometries at the B3LYP/LANL2DZ level. Chemical shifts corresponding to ^{11}B NMR were computed in relation to B_2H_6 (B3LYP shielding constant for ^{11}B NMR: 83.6 ppm) and were then converted to the standard $[\text{BF}_3\cdot\text{OEt}_2]$ scale by adding 16.6 ppm (the experimental δ (^{11}B) value of B_2H_6) to the computed values. ^1H NMR chemical shift calculations were done with TMS (SiMe_4) as the internal standard. Chemcraft [83] was used for generating orbital graphics and optimized structure plots. Natural Bond Orbital (NBO) analyses [84] allowed for arrival of the Wiberg Bond Indices (WBI) [85].

4. Conclusions

Results described in this article have demonstrated the scope of new methodologies for the synthesis of high-nuclearity cobaltaborane clusters. Firstly, one of the new routes described here has led to the isolation of a novel and unprecedented 11-vertex–12-SEP disobedient cobaltaborane cluster with a (*hyper*)*nido* M_3B_8 core. The second route has allowed for synthesis and characterization of a classic example of sequentially generated higher nuclearity cluster with a 10-vertex–12-SEP *nido* core via cluster growth on a preformed template. Indeed, cobaltaboranes and cobaltaheteroboranes constitute a showcase for dynamic and unique structural features and as a result, we are always on the lookout for possibilities of generating novel sophisticated cobaltaborane frameworks. Amongst the several synthetic strategies that are recognized in this domain, the applicability of the ones reported here may be vital and might lead to the generation of sophisticated high-nuclearity metallaborane frameworks of other group-9 metals. The unusual formation of **1** and the open-faced geometries of both **1** and **2** should imply enhanced reactivity to such species. Further efforts are currently devoted to that purpose.

Supplementary Materials: Some supplementary information is available online at www.mdpi.com/2304-6740/9/4/28/s1. It contains ^1H , $^{11}\text{B}\{^1\text{H}\}$, $^{13}\text{C}\{^1\text{H}\}$ NMR and mass spectra (Figures S1–S9); CIF and checkCIF files as well as the xyz coordinates of the DFT optimized model clusters (Figures S10–S13), selected bond parameters for clusters **1'** and **2'** and their Wiberg bond indices (WBI) (Table S1) as well as calculated HOMO and LUMO energy levels and HOMO-LUMO gaps of **1'–4'** (Table S2).

Author Contributions: K.P. and C.N. formulated and planned the experiments; K.P. and C.N. carried out the synthesis and spectroscopic analyses and discussed the results with S.G. and J.-F.H.; K.P. and C.N. organized the manuscript with guidance from S.G. and J.-F.H.; S.G. supervision, S.G. project administration. All authors have read and agreed to the published version of the manuscript.

Funding: This work was supported by CSIR (Scheme No. 01 (2939)/18/EMR-II), New Delhi, India.

Institutional Review Board Statement: Not applicable.

Informed Consent Statement: Not applicable.

Data Availability Statement: Accession codes: 2043679 (**1**), 2060786 (**2**). Crystallographic data can be acquired for free from the Cambridge Crystallographic Data Centre via www.ccdc.cam.ac.uk/data_request/cif or by emailing data_request@ccdc.cam.ac.uk, or by contacting The Cambridge Crystallographic Data Centre, 12 Union Road, Cambridge CB2 1EZ, UK; Fax: +44-1223-336033.

Acknowledgments: K.P. thanks IIT Madras and C.N. thanks the Department of Science and Technology, India, DST-INSPIRE for research fellowships. The Department of Chemistry, IIT Madras is thankfully acknowledged for X-ray support. The authors thank IIT Madras for

computational facilities and Dr. Babu Varghese and Mr. Venkatachalam Ramkumar for Single Crystal X-ray Diffraction data analyses.

Conflicts of Interest: The authors declare no conflicts of interest.

References

1. Lipscomb, W.L. *Boron Hydrides*; Benjamin: New York, NY, USA, 1963.
2. Muetterties, E.L. *Boron Hydride Chemistry*; Academic Press: New York, NY, USA, 1975.
3. Grimes, R.N. *Carboranes*, 3rd ed.; Elsevier: Oxford, UK, 2016.
4. King, R.B. Three-Dimensional Aromaticity in Polyhedral Boranes and Related Molecules. *Chem. Rev.* **2001**, *101*, 1119–1152.
5. Jemmis, E.D. Overlap control and stability of polyhedral molecules. *closo*-Carboranes. *J. Am. Chem. Soc.* **1982**, *104*, 7017–7020.
6. Hosmane, N.S.; Maguire, J.A. Metallacarboranes of d- and f-Block Metals. In *Comprehensive Organometallic Chemistry III*; Mingos, D.M.P., Crabtree, R.H., Eds.; Pergamon: New York, NY, USA, 2007; Volume 3, Chapter 3.05, pp. 175–264.
7. Hosmane, N.S. *Boron Science: New Technologies and Applications*; CRC Press, Taylor and Francis Group: Boca Raton, FL, USA, 2011.
8. Saxena, A.K.; Hosmane, N.S. Recent advances in the chemistry of carborane metal complexes incorporating d- and f-block elements. *Chem. Rev.* **1993**, *93*, 1081–1124.
9. Grimes, R.N. Transition Metal Metallacarboranes. In *Comprehensive Organometallic Chemistry II*; Abel, E.W., Stone, F.G.A., Wilkinson, G., Eds.; Pergamon Press: Oxford, UK, 1995; Volume 1, pp. 373–430.
10. Housecroft, C.E. Boron Atoms in Transition Metal Clusters. *Adv. Organomet. Chem.* **1991**, *33*, 1–50.
11. Fehlner, T.P., Halet, J.-F., Saillard, J.-Y. *Molecular Clusters. A Bridge to Solid-State Chemistry*; University Press: Cambridge, UK, 2007.
12. Zhang, J.; Xie, Z. Synthesis, structure, and reactivity of 13- and 14-Vertex Carboranes. *Acc. Chem. Res.* **2014**, *47*, 1623–1633.
13. Hawthorne, M.F.; Dunks, G.B.; McKown, M.M. Probable formation of 13-atom polyhedral complexes containing $B_{10}C_2H_{12}^{2-}$ and cobalt. *J. Am. Chem. Soc.* **1971**, *93*, 2541–2543.
14. Evans, W.J.; Hawthorne, M.F. Synthesis of fourteen vertex metallocarboranes by polyhedral expansion. *J. Chem. Soc., Chem. Commun.* **1974**, 38–39. DOI:10.1039/C39740000038.
15. Burke, A.; Ellis, D.; Giles, B.T.; Hodson, B.E.; Macgregor, S.A.; Rosair, G.M.; Welch, A.J. Beyond the Icosahedron: The First 13-Vertex Carborane. *Angew. Chem. Int. Ed.* **2003**, *42*, 225–228.
16. Deng, L.; Chan, H.-S.; Xie, Z. Synthesis, Reactivity, and Structural Characterization of a 14-Vertex Carborane. *Angew. Chem. Int. Ed.* **2005**, *44*, 2128–2131.
17. Deng, L.; Zhang, J.; Chan, H.-S.; Xie, Z. Synthesis and Structure of 14- and 15-Vertex Ruthenacarboranes. *Angew. Chem. Int. Ed.* **2006**, *45*, 4309–4313.
18. Roy, D.K.; Bose, S.K.; Anju, R.S.; Mondal, B.; Ramkumar, V.; Ghosh, S. Boron Beyond the Icosahedral Barrier: A 16-Vertex Metallaborane. *Angew. Chem. Int. Ed.* **2013**, *52*, 3222–3226.
19. Roy, D.K.; Mondal, B.; Shankhari, P.; Anju, R.S.; Geetharani, K.; Mobin, S.M.; Ghosh, S. Supraicosahedral Polyhedra in Metallaboranes: Synthesis and Structural Characterization of 12-, 15- and 16-Vertex Rhodaboranes. *Inorg. Chem.* **2013**, *52*, 6705–6712.
20. Roy, D.K.; Ghosh, S.; Halet, J.-F. Beyond the Icosahedron: The Quest for High-nuclearity Supraicosahedral Metallaboranes. *J. Clust. Sci.* **2014**, *25*, 225–237.
21. Onak, T. Polyhedral Carboranes. In *Comprehensive Organometallic Chemistry II*; Abel, E.W., Stone, F.G.A., Wilkinson, G., Eds.; Pergamon Press: Oxford, UK, 1995; Chapter 6, Volume 1, p. 217–255.
22. Hosmane, N.S.; Siebert, W. (Eds.) *Advances in Boron Chemistry*; Royal Society of Chemistry: Cambridge, UK, 1997; p. 349.
23. Ghosh, S.; Rheingold, A.L.; Fehlner, T.P. Metallaboranes of the Earlier Transition Metals. An Arachno Nine-vertex, Nine-Skeletal Electron Pair Rhenaborane of Novel Shape: Importance of Total Vertex Connectivities in Such Systems. *Chem. Commun.* **2001**, *10*, 895–896.
24. Ghosh, S.; Lei, X.; Shang, M.; Fehlner, T.P. Role of the Transition Metal in Metallaborane Chemistry. Reactivity of $[(Cp^*ReH_2)_2B_4H_4]$ with $BH_3 \cdot THF$, CO, and $[Co_2(CO)_8]$. *Inorg. Chem.* **2000**, *39*, 5373–5382.
25. Ghosh, S.; Noll, B.C.; Fehlner, T.P. Borane Mimics of Classic Organometallic Compounds: $[(Cp^*Ru)B_8H_{14}(RuCp^*)]^{0+}$, Isoelectronic Analogues of Dinuclear Pentalene Complexes. *Angew. Chem. Int. Ed.* **2005**, *44*, 6568–6571.
26. Ghosh, S.; Fehlner, T.P.; Noll, B.C. Condensed metallaborane clusters: Synthesis and structure of $Fe_2(CO)_6(\eta^5-C_5Me_5RuCO)(\eta^5-C_5Me_5Ru)B_6H_{10}$. *Chem. Commun.* **2005**, 3080–3082. DOI:10.1039/B502559A.
27. Ghosh, S.; Noll, B.C.; Fehlner, T.P. Expansion of Iridaborane Clusters by Addition of Monoborane. Novel Metallaboranes and Mechanistic Detail. *Dalton Trans.* **2008**, *3*, 371–378.
28. Geetharani, K.; Bose, S.K.; Pramanik, G.; Saha, T.K.; Ramkumar, V.; Ghosh, S. An Efficient Route to Group 6 and 8 Metallaborane Compounds: Synthesis of *arachno*- $[Cp^*Fe(CO)B_3H_8]$ and *closo*- $[(Cp^*M)_2B_3H_9]$ (M = Mo, W). *Eur. J. Inorg. Chem.* **2009**, *2009*, 1483–1487.
29. Dhayal, R.S.; Sahoo, S.; Reddy, K.H.K.; Mobin, S.M.; Jemmis, E.D.; Ghosh, S. Vertex-Fused Metallaborane Clusters: Synthesis, Characterization and Electronic Structure of $[(\eta^5-C_5Me_5Mo)_3MoB_9H_{18}]$. *Inorg. Chem.* **2010**, *49*, 900–904.

30. Geetharani, K.; Bose, S.K.; Sahoo, S.; Varghese, B.; Mobin, S.M.; Ghosh, S. Cluster Expansion Reactions of Group 6 and 8 Metallaboranes Using Transition Metal Carbonyl Compounds of Groups 7-9. *Inorg. Chem.* **2011**, *50*, 5824–5832.
31. Chakrahari, K.K.V.; Thakur, A.; Mondal, B.; Dhayal, R.S.; Ramkumar, V.; Ghosh, S. A Close-packed Boron-rich 11-vertex Molybdaborane with Novel Geometry. *J. Organomet. Chem.* **2012**, *710*, 75–79.
32. Roy, D.K.; Barik, S.K.; Mondal, B.; Varghese, B.; Ghosh, S. A Novel Heterometallic μ^9 -Boride Cluster: Synthesis and Structural Characterization of $[(\eta^5\text{-C}_5\text{Me}_5\text{Rh})_2\{\text{Co}_6(\text{CO})_{12}\}(\mu\text{-H})(\text{BH})\text{B}]$. *Inorg. Chem.* **2014**, *53*, 667–669.
33. De, A.; Zhang, Q.-F.; Mondal, B.; Cheung, L.F.; Kar, S.; Saha, K.; Varghese, B.; Wang, L.-S.; Ghosh, S. $[(\text{Cp}^*\text{M})_2\text{B}_9\text{H}_{11}]$ (M = Zr or Hf): Early Transition Metal ‘guarded’ Heptaborane with Strong Covalent and Electrostatic Bonding. *Chem. Sci.* **2018**, *9*, 1976–1981.
34. Bould, J.; Rath, N.P.; Barton, L. Metallaborane heteroatom incorporation reactions: Metallacarboranes, metallathiaboranes, and an iridaazaborane from iridanonaborane precursors. *Organometallics* **1996**, *15*, 4916–4929.
35. Ferguson, G.; Lough, A.J.; Faridooon; McGrath, M.N.; Spalding, T.R.; Kennedy, J.D., Fontaine, X.L.R. Metallaheteroborane chemistry. Part 7. Synthesis, crystal structure, and characterisation of two dinuclear rhodotelluraboranes, $[(\text{PPh}_3)_2\text{RhTeB}_{10}\text{H}_{10}]_2$ and $[(\text{PPh}_3)(\text{CO})\text{RhTe}_2\text{B}_{20}\text{H}_{20}]$. *J. Chem. Soc. Dalton Trans.* **1990**, *6*, 1831–1839.
36. Ferguson, G.; Gallagher, J.F.; McGrath, M.; Sheehan, J.P.; Spalding, T.R.; Kennedy, J.D. Metallaheteroborane chemistry. Part 11. Selective syntheses of the palladium heteroborane complexes $[2,2\text{-}(\text{PR}_3)_2\text{-closo-}2,1\text{-PdEB}_{10}\text{H}_{10}]$ ($\text{R}_3 = \text{Ph}_3, \text{MePh}_2$ or Me_2Ph ; E = Se or Te) and $[2\text{-X-}2\text{-}(\text{PPh}_3)\text{-closo-}2,1\text{-PdTeB}_{10}\text{H}_9(\text{PPh}_3)]$ (X = Cl, Br, I, CN, SCN or O_2CMe). *J. Chem. Soc. Dalton Trans.* **1993**, *1*, 27–34.
37. Norman, N.C.; Orpen, A.G.; Quayle, M.J.; Rice, C.R. Diborane(4) compounds incorporating thio- and seleno-carboranyl groups. *New J. Chem.* **2000**, *24*, 837–839.
38. Hammerschmidt, A.; Doch, M.; Putz, S.; Krebs, B. $\text{Na}_2[\text{B}_{18}\text{Se}_{16}]$: The first 3D polymeric selenoborato-closo-dodecaborate. *Z. Anorg. Allg. Chem.* **2005**, *631*, 1125–1128.
39. Ferguson, G.; Gallagher, J.F.; Kennedy, J.D.; Kelleher, A.M.; Spalding, T.R. Pentahapto-bonded gold heteroborane clusters $[3\text{-}(\text{R}_3\text{P})\text{-closo-}2,1\text{-AuTeB}_{10}\text{H}_{10}]^-$ and $[3\text{-}(\text{R}_3\text{P})\text{-closo-}3,1,2\text{-AuAs}_2\text{B}_9\text{H}_9]^-$. *Dalton Trans.* **2006**, *7*, 2133–2139.
40. Bose, S.K.; Geetharani, K.; Ramkumar, V.; Varghese, B.; Ghosh, S. Chemistry of vanadaboranes: Synthesis, structures and characterization of organ vanadium sulfide clusters with disulfide linkage. *Inorg. Chem.* **2010**, *49*, 2881–2888.
41. Ghosh, S.; Noll, B.C.; Fehlner, T.P. Synthesis and characterization of $[\text{exo-BH}_2(\text{Cp}^*\text{M})_2\text{B}_9\text{H}_{14}]$ (M = Ru, Re), and the conversion of the ruthenaborane into $[(\text{Cp}^*\text{Ru})_2\text{B}_{10}\text{H}_{16}]$ with an open cluster framework based on a capped truncated tetrahedron. *Angew. Chem. Int. Ed.* **2005**, *44*, 2916–2918.
42. Ghosh, S.; Shang, M.; Fehlner, T.P. Comparison of the geometric and molecular orbital structures of $(\text{Cp}^*\text{Cr})_2\text{B}_4\text{H}_8$ and $(\text{Cp}^*\text{Re})_2\text{B}_4\text{H}_8$, $\text{Cp}^* = \eta^5\text{-C}_5\text{Me}_5$. Structural consequences of delocalized electronic unsaturation in a metallaborane cluster. *J. Organomet. Chem.* **2000**, *614*, 92–98.
43. Geetharani, K.; Bose, S.K.; Varghese, B.; Ghosh, S. From metallaborane to borylene complexes: Syntheses and structures of triply bridged ruthenium and tantalum borylene complexes. *Chem. Eur. J.* **2010**, *16*, 11357–11366.
44. Bose, S.K.; Ghosh, S.; Noll, B.C.; Halet, J.-F.; Saillard, J.-Y.; Vega, A. Linked and fused tungstaborane clusters: Synthesis, characterization and electronic structures of bis- $\{(\eta^5\text{-C}_5\text{Me}_5\text{W})_2\text{B}_3\text{H}_3\}_2$ and $(\eta^5\text{-C}_5\text{Me}_5\text{W})_2\{\text{Fe}(\text{CO})_3\}_n\text{B}_{6-n}\text{H}_{10-n}$, n = 0,1. *Organometallics* **2007**, *26*, 5377–5385.
45. Ghosh, S.; Lei, X.; Cahill, C.L.; Fehlner, T.P. Symmetrical scission of the coordinated tetraborane in $(\text{Cp}^*\text{ReH}_2)_4\text{B}_4\text{H}_4$ on CO addition and reassociation of the coordinated diboranes on H_2 loss. *Angew. Chem. Int. Ed.* **2000**, *39*, 2900–2902.
46. Zafar, M.; Kar, S.; Nandi, C.; Ramalakshmi, R.; Ghosh, S. Cluster Fusion: Face-Fused Macropolyhedral Tetracobaltaboranes. *Inorg. Chem.* **2019**, *58*, 47–51.
47. Venable, T.L.; Sinn, E.; Grimes, R.N. Cobaltaborane analogs of decaborane ($\text{B}_{10}\text{H}_{14}$). Crystal and molecular structures of 6- $[\eta^5\text{-C}_5(\text{CH}_3)_5]\text{CoB}_9\text{H}_{13}$, 6,9- $[\eta^5\text{-C}_5(\text{CH}_3)_5]_2\text{Co}_2\text{B}_8\text{H}_{12}$, 5,7- $[\eta^5\text{-C}_5(\text{CH}_3)_5]_2\text{Co}_2\text{B}_8\text{H}_{12}$, and 6-Cl-5,7- $[\eta^5\text{-C}_5(\text{CH}_3)_5]_2\text{Co}_2\text{B}_8\text{H}_{11}$. *Inorg. Chem.* **1982**, *21*, 895–904.
48. Venable, T.L.; Grimes, R.N. (Pentamethylcyclopentadienyl)-cobaltaboranes derived from the octah dropentaborate (B_5H_8^-) and tetradecahydrononaborate ($\text{B}_9\text{H}_{14}^-$) ions: Studies in synthesis and structure. *Inorg. Chem.* **1982**, *21*, 887–892.
49. Pipal, J.R.; Grimes, R.N. Crystal structure of a tetracobalt tetraboron cluster, $(\eta^5\text{-C}_5\text{H}_5)_4\text{Co}_4\text{B}_4\text{H}_4$. Structural patterns in eight-vertex polyhedra. *Inorg. Chem.* **1979**, *18*, 257–263.
50. Chakrahari, K.K.; Sharmila, D.; Barik, S.K.; Mondal, B.; Varghese, B.; Ghosh, S. Hypoelectronic metallaboranes: Synthesis, structural characterization and electronic structures of metal-rich cobaltaboranes. *J. Organomet. Chem.* **2014**, *749*, 188–196.
51. Barik, S.K.; Roy, D.K.; Sharmila, D.; Ramalakshmi, R.; Chakrahari, K.K.; Mobin, S.M.; Ghosh, S.; Synthesis, Characterization and Electronic Structures of Rh and Co analogs of Decaborane-14. *Proc. Natl. Acad. Sci. India Sect. A* **2014**, *84*, 121–130.
52. Barik, S.K.; Roy, D.K.; Ghosh, S. Chemistry of group 9 dimetallaborane analogues of octaborane(12). *Dalton Trans.* **2015**, *44*, 669–676.
53. Roy, D.K.; Anju, R.S.; Varghese, B.; Ghosh, S. Reactivity of dirhodium analogs of octaborane-12 and decaborane-14 toward transition-metal moieties. *Organometallics* **2013**, *32*, 1964–1970.
54. Nandi, C.; Kar, S.; Zafar, M.; Kar, K.; Ghosh, S. Chemistry of Dimetalla octaborane(12) with Chalcogen-Based Borate Ligands: Obedient versus Disobedient Clusters. *Inorg. Chem.* **2020**, *59*, 3537–3541.
55. Roy, D.K.; Bose, S.K.; Anju, R.S.; Ramkumar, V.; Ghosh, S. Synthesis and Structure of Dirhodium Analogue of Octaborane-12 and Decaborane-14. *Inorg. Chem.* **2012**, *51*, 10715–10722.

56. Stibr, B.; Holub, J.; Bakardjiev, M.; Hnyk, D.; Tok, O.L.; Milius, W.; Wrackmeyer, B. Phosphacarborane Chemistry: The Synthesis of the Parent Phosphadecaboranes *nido*-7,8,9-PC₂B₈H₁₁ and [*nido*-7,8,9-PC₂B₈H₁₀]⁻, and Their 10-Cl Derivatives-Analogs of the Cyclopentadienide Anion. *Eur. J. Inorg. Chem.* **2002**, *2002*, 2320–2326.
57. Volkov, O.; Macias, R.; Rath, N.P.; Barton, L. Phosphine–Boranes as Bidentate Ligands: Formation of [8,8- η^2 -{ η^2 -(BH₃)-dppm}-*nido*-8,7-RhSB₉H₁₀] and [9,9- η^2 -{ η^2 -(BH₃)-dppm}-*nido*-9,7,8-RhC₂B₈H₁₁] from [8,8-(η^2 -dppm)-8-(η^1 -dppm)-*nido*-8,7-RhSB₉H₁₀] and [9,9-(η^2 -dppm)-9-(η^1 -dppm)-*nido*-9,7,8-RhC₂B₈H₁₁], Respectively. *Inorg. Chem.* **2002**, *41*, 5837–5843.
58. Dou, J.; Wu, L.; Guo, Q.; Li, D.; Wang, D. A New Strategy for the Preparation of Metallaboranes-Solvolothermal Synthesis and Structural Characterisation of Two Nido 11-vertex Diplatinoundecaborane Clusters. *Eur. J. Inorg. Chem.* **2005**, *2005*, 63–65.
59. Mingos, D.M.P. Polyhedral skeletal electron pair approach. *Acc. Chem. Res.* **1984**, *17*, 311–319.
60. Jung, C.W.; Hawthorne, M.F. Eleven-Vertex Rhodium, Iridium, and Ruthenium Phosphinometalloborane Complexes Formed from Sodium Undecahydro-5,6-dicarba-*nido*-decaborate (1-). *J. Am. Chem. Soc.* **1980**, *102*, 3024–3032.
61. Ferguson, G.; Jennings, M.C.; Lough, A.J.; Coughlan, S.; Spalding, T.R.; Kennedy, J.D.; Fontaine, X.L.R.; Stibr, B. Novel Rhodathiaborane Complexes Derived from [(PPh₃)₂RhSB₉H₁₀]. *J. Chem. Soc. Chem. Commun.* **1990**, *12*, 891–894.
62. Coughlan, S.; Spalding, T.R.; Ferguson, G.; Gallagher, J.F.; Lough, A.J.; Fontaine, X.L.R.; Kennedy, J.D.; Stibr, B. Metallaheteroborane chemistry. Part 10. Synthesis and characterisation of *closo*-structured rhodathiaborane complexes [1-(CO)-1-L-3-L'-1,2-RhSB₉H₈](L = L' = PPh₃; L = PMe₂Ph, L' = PMe₂Ph or PPh₃). *J. Chem. Soc. Dalton Trans.* **1992**, *19*, 2865–2871.
63. Volkov, O.; Macias, R.; Rath, N.P.; Barton, L. Chemistry on a metallathiaborane cluster Part 4: Reactions of 11-vertex rhodathiaboranes with bidentate phosphines and their subsequent rearrangements. *J. Organomet. Chem.* **2002**, *657*, 40–47.
64. Volkov, O.; Rath, N.P.; Barton, L. Chemistry of a Metallathiaborane Cluster. 5. Reaction of [8,8-(η^2 -dppm)-8-(η^1 -dppm)-*nido*-8,7-RhSB₉H₁₀] and Its Derivatives with Organotransition-Metal Reagents. *Organometallics* **2002**, *21*, 5505–5514.
65. Bould, J.; Cunchillos, C.; Lahoz, F.J.; Oro, L.A.; Kennedy, J.D.; Macias, R. New Iridathiaboranes with Reversible *Isonido*–*Nido* Cluster Flexibility. *Inorg. Chem.* **2010**, *49*, 7353–7361.
66. Kasper, J.S.; Lucht, C.M.; Harker, D. The Crystal Structure of Decaborane, B₁₀H₁₄. *Acta Cryst.* **1950**, *3*, 436–455.
67. Kölle, U.; Khouzami, F.; Fuss, B. Bridged C₅Me₃Co^{II} Complexes—Reactive Intermediates in the Cyclopentadienylation of Cobalt(II) Halides. *Angew. Chem. Int. Ed.* **1982**, *21*, 131–132.
68. Yoshino, T.; Ikemoto, H.; Matsunaga, S.; Kanai, M.A. Cationic High-Valent Cp*Co^{III} Complex for the Catalytic Generation of Nucleophilic Organometallic Species: Directed C–H Bond Activation. *Angew. Chem. Int. Ed.* **2013**, *52*, 2207–2211.
69. Lalancette, J.M.; Frêche, A.; Monteux, R. Reductions with sulfurated borohydrides. I. Preparation of sulfurated borohydrides. *Can. J. Chem.* **1968**, *46*, 2754–2757.
70. Lalancette, J.M.; Arnac, M. Reductions with sulfurated borohydrides. III. Borohydrides incorporating selenium and tellurium. *Can. J. Chem.* **1969**, *47*, 3695–3697.
71. Ryschkewitsch, G.E.; Nainan, K.C. Octahydrotriborate(1-) ([B₃H₈]⁻) salts. Method A. *Inorg. Synth.* **1974**, *15*, 113–114.
72. Altomare, A.; Cascarano, G.; Giacovazzo, C.; Guagliardi, A.; Burla, M.C.; Polidori, G.; Camalli, M. SIRPOW. 92—A program for automatic solution of crystal structures by direct methods optimized for powder data. *J. Appl. Cryst.* **1994**, *27*, 435–436.
73. Sheldrick, G.M. SHELXT—Crystal structure refinement with SHELXL. *Acta Cryst.* **2015**, *71*, 3–8.
74. Sheldrick, G.M. *SHELXS97 and SHELXL97: Program for Crystal Structure Solution and Refinement*; University of Gottingen: Gottingen, Germany, 1997.
75. Dolomanov, O.V.; Bourhis, L.J.; Gildea, R.J.; Howard, J.A.K.; Puschmann, H. OLEX2: A complete structure solution, refinement and analysis program. *J. Appl. Cryst.* **2009**, *42*, 339–341.
76. Frisch, M.J.; Trucks, G.W.; Schlegel, H.B.; Scuseria, G.E.; Robb, M.A.; Cheeseman, J.R.G.; Mennucci, B.; Petersson, G.A.; Nakatsuji, H.; Caricato, M.; et al. *Gaussian 09, Revision C.01*; Gaussian, Inc.: Wallingford, CT, USA, 2010.
77. Lee, C.; Yang, W.; Parr, R.G. Development of the Colic-Salvetti correlation-energy formula into a functional of the electron density. *Phys. Rev. B* **1988**, *37*, 785–789.
78. Wadt, W.R.; Hay, P.J. *Ab Initio* effective core potentials for molecular calculations. Potentials for the transition metal atoms Sc to Hg. *J. Chem. Phys.* **1985**, *82*, 270–283.
79. Pritchard, B.P.; Altarawy, D.; Didier, B.; Gibson, T.D.; Windus, T.L. A New Basis Set Exchange: An Open, Up-to-date Resource for the Molecular Sciences Community. *J. Chem. Inf. Model.* **2019**, *59*, 4814–4820.
80. London, F.J. Quantum theory of interatomic currents in aromatic combinations. *J. Phys. Radium* **1937**, *8*, 397–409.
81. Ditchfield, R. Self-consistent perturbation theory of diamagnetism. *Mol. Phys.* **1974**, *27*, 789–807.
82. Wolinski, K.; Hinton, J.F.; Pulay, P. Efficient implementation of the gauge-independent atomic orbital method for NMR chemical shift calculations. *J. Am. Chem. Soc.* **1990**, *112*, 8251–8260.
83. Chemcraft-Graphical Software for Visualization of Quantum Chemistry Computations. Available online: <https://www.chemcraftprog.com> (accessed on 21 March 2021).
84. Glendening, E.D.; Badenhoop, J.K.; Reed, A.E.; Carpenter, J.E.; Bohmann, J.A.; Morales, C.M.; Landis, C.R.; Weinhold, F. *NBO Program 6.0*; Theoretical Chemistry Institute, University of Wisconsin: Madison, WI, USA, 2013.
85. Wiberg, K. Application of the Pople-Santry-Segal CNDO Method to the Cyclopropylcarbonyl and Cyclobutyl Cation and to Bicyclobutane. *Tetrahedron* **1968**, *24*, 1083–1096.